EMERGING TOPICS
PHYSIOLOGY 22: 358–365, 2007; 10.1152/physiol.00032.2007

In Vivo Calcium Imaging of Neural Network Function

Werner Göbel and Fritjof Helmchen
Department of Neurophysiology, Brain Research Institute, University of Zurich, Zurich, Switzerland
goebel@hifo.uzh.ch

Spatiotemporal activity patterns in local neural networks are fundamental to brain function. Network activity can now be measured in vivo using two-photon imaging of cell populations that are labeled with fluorescent calcium indicators. In this review, we discuss basic aspects of in vivo calcium imaging and highlight recent developments that will help to uncover operating principles of neural circuits.

In the nervous system, all sensations and behaviors are encoded in dynamic patterns of activity in cellular networks. Through a sequence of neural networks, sensory information is transmitted to higher, associative brain areas. Following integration in these areas, specific activity patterns are eventually formed in the relevant motoneuron pools to produce adequate behavior. In this chain of events, key processing steps are thought to occur on the level of local microcircuits that contain on the order of 1,000–10,000 cells. These local circuits form highly connected three-dimensional networks that, other than the projection neurons, typically contain various inhibitory and excitatory interneuron types. In addition, neuronal networks form dense meshworks with the surrounding glial cells.

Despite the fundamental importance of microcircuits, their operating principles remain enigmatic. How local networks process incoming signals and integrate them with ongoing brain activity is poorly understood. The reason is that experimental tools to record from large sets of neurons in the living brain (in vivo) are still limited. Although multi-electrode extracellular recordings enable simultaneous recordings from hundreds of neurons in behaving animals (6), such recordings sample from widely distributed cell populations with poorly defined cell types and spatial relationships. As an alternative and complimentary technique, two-photon laser scanning microscopy (2PLSM) (7) enables high-resolution functional imaging in living animals. Providing a depth penetration of several hundred microns in intact tissue, 2PLSM is excellently suited to study structure and function of cells and networks within their native environment. For details on principles of 2PLSM and recent applications, see Refs. 11, 19, 54, 66.

Here, we focus on in vivo two-photon imaging as an emerging technique to reveal activity patterns in local networks of the mammalian brain. Novel methods to stain populations of cells with activity-dependent fluorescent markers, in particular calcium-sensitive indicators (17, 18, 33, 34, 51), have opened the door for comprehensive studies of the functional organization of microcircuits. We first introduce the basics of population calcium imaging, including labeling and fluorescence read-out methods.

Calcium Indicator Labeling

Two-photon imaging relies on fluorescence excitation and, in general, necessitates staining of cells with fluorescent dyes. Various staining methods have been developed for in vivo calcium measurements. Single cells can be filled with membrane-impermeable calcium indicators via intracellular recording electrodes (22, 53) or by single-cell electroporation (34). In addition, several methods are available for labeling of cell populations. Injection of dextran-conjugated forms of organic calcium indicators (e.g., calcium green-1 dextran) into axonal pathways leads to local dye uptake with subsequent anterograde and retrograde transport over hours and days (13, 39) (FIGURE 1A). In the mammalian brain, this method has been applied to measure calcium signals in afferent axonal terminals in vivo (29, 61) and in retrogradely labeled neuronal populations in spinal cord and retina in vitro (38, 63).

Groups of 10-100 neurons can be loaded in vivo by using either targeted electroporation (34) or local electroporation, as recently demonstrated for mouse neocortex, olfactory bulb, and cerebellum (33) (FIGURE 1B). In the latter case, a micropipette containing a high concentration of calcium indicator in salt-form or as dextran-conjugate is inserted into the target area but is not particularly aimed at a specific cell. Mild electrical pulses are applied through the micropipette, causing transient membrane disruptions in nearby neuronal dendrites and dye uptake. Following many repetitions, dye has accumulated intracellularly and diffused throughout the affected cells. An advantage of the resulting sparse labeling is that subcellular calcium signals can be resolved in dendrites and synaptic structures because of the low background staining (33).

Large-scale in vivo staining of entire cell populations can be achieved using membrane-permeable acetoxymethyl (AM) ester forms of calcium indicators (60) (FIGURE 1C). Following diffusion through the cell membrane, the ester groups are cleaved by cytosolic esterases so that the dye molecules, now membrane impermeable, are trapped inside the cells. AM ester loading has been long applied in cell cultures and in brain slices. Successful in vivo loading eventually was achieved by bolus injection of the AM ester dye into the brain (51). This "multi-cell bolus loading" (MCBL) technique at present is the

1548-9213/05 8.00

most commonly used in vivo network labeling approach and has been applied to a number of brain areas in various animal species (5, 26, 36, 40, 52). A detailed protocol for MCBL can be found in Ref. 12.

An alternative to "traditional" organic dyes are genetically encoded calcium indicators (GECIs) (for reviews, see Refs. 10, 27, 28, 31). GECIs are calcium-sensitive fluorescent proteins that can be expressed in subsets of cells in transgenic animals using specific promoters (8, 17, 18) (FIGURE 1D). Although traditional high-affinity calcium indicators still are superior to GECIs in some respects (42), the sensitivity of GECIs is continually improving. Meanwhile, somatic calcium signals evoked by only a few action potentials (APs), as well as dendritic calcium signals, can be detected in vivo (18).

To understand the function of a neural circuit, one would like to discriminate its sub-network components. To this end, counterstaining of specific cell types has proven helpful, especially in bulk loaded tissue where markers need not be calcium sensitive (FIGURE 1E). In rodents, cortical astrocytes are identified with the red fluorescent dye sulforhodamine 101 (37). In addition, transgenic mice with fluorescent protein expression in specific neuronal subsets, e.g., in GABAergic interneurons (57), allow separation of functional signals into different neuronal subtypes (50). For the future, we can expect transgenic animals with colourful co-expression of different GECIs in the various cellular sub-networks.

Network Scanning Approaches

The new options for in vivo population labeling pose a challenge for 2PLSM in terms of reading out network dynamics. Simultaneous sampling of neuronal calcium signals (typically 0.5-1 s long) in hundreds of cells with sufficient temporal resolution is not trivial. In the standard imaging mode, the laser focus is scanned within one focal plane in a raster-like fashion (FIGURE 2A). In this raster mode, the data acquisition rate (for the individual cells) is determined by the rate at which the entire scan pattern is repeated. Consequently, imaging of large fields is slow. Moreover, the choice of cells is somewhat random, and not all cells can be optimally in focus. More flexibility is achieved by rotation of the image plane using focusing devices appropriate for rapid *z*-scanning (14, 35), for example piezo-electric focusing elements that can drive microscope objective movements at rates of 10 Hz and more (FIGURE 2B).

Entirely new scanning approaches are required for fast network measurements in 3D space, taking into account the 3D structure of neural circuits. The simplest option is 2D raster scanning while continuously moving the objective (FIGURE 2C) (16). Acquisition rates in this mode typically are limited to <1 Hz, and valuable scan time is wasted on background structures. Fast scanning systems using resonant scanners or acousto-optical devices (AODs) could further increase 3D acquisition rates.

More easily, rapid scanning in 3D (with rates of 10 Hz and higher) is achieved with non-raster-like scan patterns (FIGURE 2, D–F). For instance, a closed scan trajectory in 3D space can be generated by applying appropriate signals to the *xy*-scan mirrors while rapidly scanning along the optical axis with a piezo-electric focusing element (15). Such a 3D line scan can be defined by analytical functions, but it can also be trimmed to include specific user-defined points of interest such as cell bodies (FIGURE 2E). As we recently could demonstrate for neocortical networks in vivo, calcium

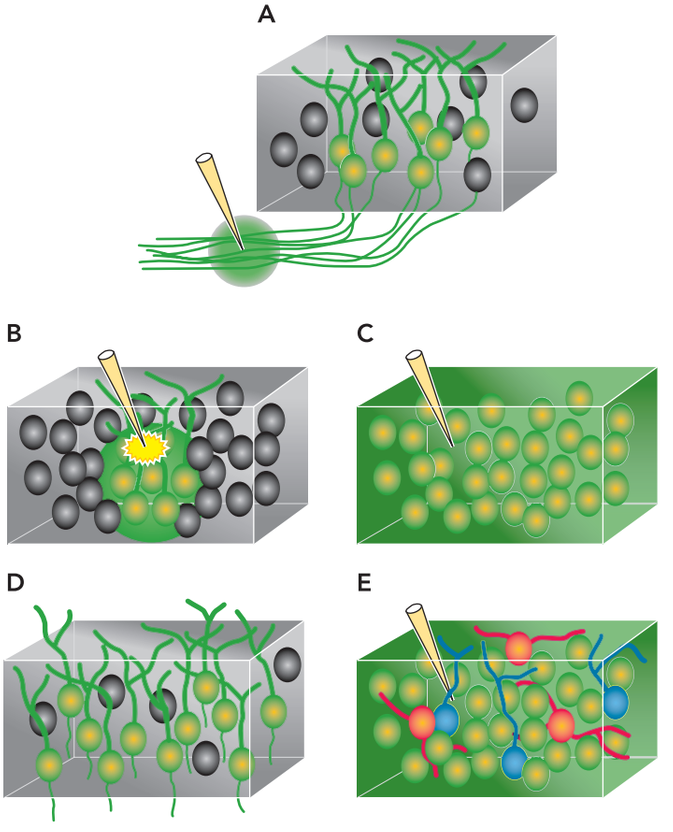

FIGURE 1. **In vivo labeling of cellular networks with calcium indicator**
A: retrograde labeling using dextran-conjugated calcium-sensitive dye. *B*: labeling of a subset of cells using local electroporation. *C*: multi-cell bolus loading (MCBL) by injection of AM-ester calcium indicator results in unspecific labeling of cell somata and a diffuse background in the neuropil. *D*: expression of a genetically encoded calcium indicator (GECI) in a particular cell type. *E*: multicolor labeling by combining MCBL with specific counterstains. Various fluorescent dyes can help to distinguish neuronal and glial networks and identify neuronal sub-networks.

signals can be sampled from hundreds of cells with nearly 100% of cells "hit" in tissue cubes of 0.25-mm side length (15).

Finally, novel ways to deflect the laser beam discontinuously promise to enable 3D random-access scanning, which effectively means to "jump" from cell to cell (FIGURE 2F). Possible implementations are AOD-based random-access scanning in 2D (24, 47) combined with fast *z*-scanning (15, 16, 35), special arrangements of multiple AODs for inertia-free scanning in 3D (44), or laser illumination through optical fibers with their tips suitably positioned to direct the laser focus to pre-defined locations (46). Assuming point-to-point transition times of around 10 μs, one can imagine 3D measurements from 1,000 cells with 100-Hz resolution. Taken together, all these developments greatly extend the possibilities for in vivo optical recordings of the functional organization of neural circuits.

Calcium Signaling in Various Cellular Structures

We now take a closer look at the origin, analysis, and optimization of fluorescence signals. Various signal components may be present, especially in the case of MCBL where not only cell bodies are stained but also neuropil structures including axonal, dendritic, and glial processes (FIGURE 3, A AND B). Distinct calcium signals are observed in the various tissue compartments as we illustrate here using simulated artificial data.

Neuronal signals

Due to the presence of voltage-gated calcium channels in neuronal membranes, each AP causes a brief (around 1 ms) calcium influx (3). The resulting transient elevations of the intracellular calcium concentration above resting level (so-called "calcium transients", Δ[Ca]) typically display a sharp rise followed by an exponential decay with a time constant of around 0.5-1 s for neuronal somata (FIGURE 3C). So far, AP-evoked calcium transients are the predominant signals observed in vivo, although subthreshold neuronal activation may also lead to either highly localized or more widespread calcium signals (30, 45). Here, we presume AP-evoked calcium influx as the only source so that population spiking activity can be indirectly inferred from the somatic calcium signals (26, 49, 51, 64) (see also below). Using this approach, the microanatomical organization of sensory-evoked population responses has been mapped, for example, in the primary visual cortex of rodents and cats (32, 40, 41, 50), in rodent barrel cortex (25, 48), and in zebrafish olfactory bulb and optic tectum (36, 64, 65). With a high-affinity indicator such as Oregon Green BAPTA-1, even single APs can be optically detected (26).

Calcium signaling in glial networks

Glia cells are electrically mostly silent and, therefore, difficult to investigate in vivo by electrophysiological means. All the more in vivo imaging of calcium signalling in glial cells has gained particular interest during recent years, e.g., to clarify the function of astrocytes in local neocortical networks (59). Astrocytic calcium signals have a much slower, wave-like time course (23, 37) (FIGURE 3C). They are linked to the regulation of cerebral blood flow (56) and show altered properties in models of epilepsy (58) and Alzheimer's disease (55). Finally, sensory-evoked astrocytic calcium signals (62) suggest participation of the astrocytic network in local network processing.

Neuropil calcium signals

In several studies employing MCBL, calcium signals have been observed in the diffusely stained neuropil, both during spontaneous activity and in response to sensory stimulation (26, 40, 41, 48, 50). The neuropil signal represents an average signal from many densely packed cellular processes, and spontaneous signals were found to strongly correlate with the electrocorticogram, thus providing an "optical encephalogram" (OEG) (26). Because neuropil calcium signals are not affected in amplitude by locally blocking synaptic transmission and since dendrites contribute little (26), neuropil signals most likely originate primarily from calcium influx into presynaptic boutons and adjacent axonal segments. Hence, they reflect afferent synaptic input, which makes it possible to study

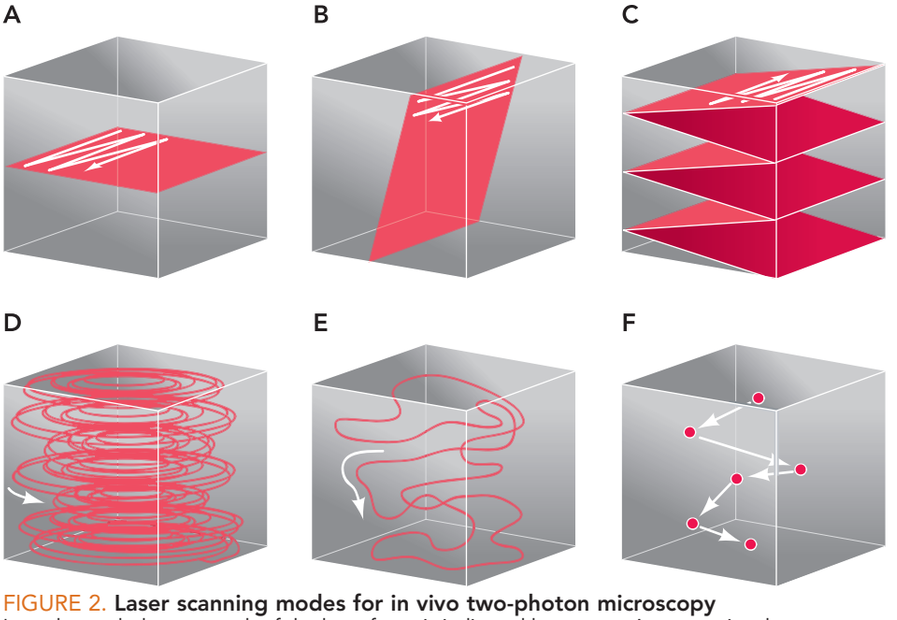

FIGURE 2. **Laser scanning modes for in vivo two-photon microscopy**
In each panel, the scan path of the laser focus is indicated by arrows. *A*: conventional raster scan in a single focal plane. *B*: with a fast *z*-scanning device, the image plane can be tilted. *C*: back-and-forth raster scan in 3D. *D*: 3D line scan employing an analytical function for the *xy*-deflection (in this case, an opening and closing spiral pattern). *E*: user-defined 3D scan trajectory. *F*: principal idea of 3D random-access scanning by discontinuous displacements of the laser focus in 3D.

input-output relationships of local circuits in a purely optical manner (26).

In general, the calcium signals in the various cellular structures translate into noisy fluorescence measurements (FIGURE 3D). In addition, some mixing of fluorescence signals between structures may occur in the microscope, as will be discussed further below. Noise in the best case is limited by shot noise, which is due to the statistical fluctuations in the detected photon counts. Additional noise sources include signal detection electronics and tissue movements. Noise is most confounding for the detection of small calcium transients like those that occur during spiking activity in neuronal somata. We therefore consider this case in more detail.

Optical Detection of Neuronal Spikes

Assuming APs as the only trigger of calcium influx, spike patterns are directly reflected in the trains of calcium transients. Mathematically speaking, each fluorescence trace is the convolution of the spike train with the single AP-evoked calcium transient plus added noise (FIGURE 4A). The challenge is to reconstruct spike patterns from the noisy traces, which can be done, for example, by using template-matching routines (26, 50), by calculating the first derivative of the fluorescence signals and threshold application (43, 49), or with deconvolution methods (64). Note that the temporal resolution will be limited by the acquisition rate of the network scanning approach. In addition, the signal-to-noise ratio (SNR) of fluorescence signals will be a decisive factor for the accuracy of the reconstruction. Here, some basic considerations may help to optimize signal conditions.

Single AP-evoked calcium transients depend on a number of factors and may differ for different cell types. For example, although single AP-evoked calcium transients can be resolved in pyramidal cells (26), it is not clear whether they are detectable in fast-spiking interneurons in vivo. The amplitude Δ[Ca] depends on the amount of calcium entry per AP, which is determined by channel expression and AP width, whereas the time constant τ depends on the calcium extrusion mechanisms present. Both amplitude and time course are also affected by the calcium indicator. Because the dye acts as an additional calcium buffer, calcium transients are reduced and prolonged with increasing dye concentration. The magnitude of this effect depends on the relative amounts of the calcium buffering capacity of the indicator dye (κ_{dye}) and the calcium buffering capacity of endogenous calcium-binding proteins (κ_s) (21). Buffering capacity is here defined as the ratio of the change in buffer-bound calcium and the change in

"Distinct calcium signals are observed in the various tissue compartments."

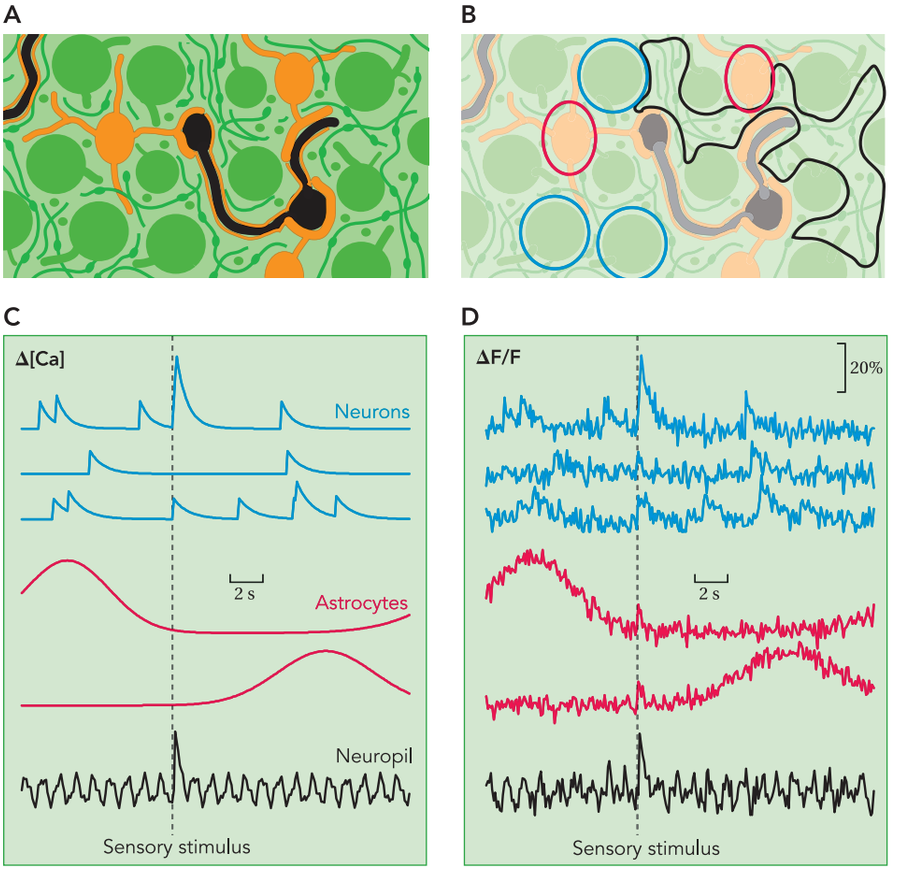

FIGURE 3. **Signal components in bulk-loaded neocortical network**
A: schematic of cellular structures labeled with MCBL. Other than cell bodies of neurons (green) and SR101-counterstained astrocytes (orange), cellular processes are stained in the neuropil, which includes dendrites as well as axons with presynaptic boutons. *B*: regions-of-interest (ROIs) selected from three neurons (blue), two astrocytes (red), and the neuropil (black). *C*: illustration of typical calcium signals in the various cellular structures using artificially generated data. Neuronal calcium transients reflect underlying spiking activity (*top*), whereas astrocytes show calcium waves on a longer time scale (*middle*). In the neuropil, fluctuations of the mean calcium signal are observed, which during anaesthesia are linked to cortical up and down states (*bottom*). All structures show spontaneous activity in vivo and may respond to sensory stimulation. *D*: calcium signals translate into fluorescence signals, which typically are expressed as relative fluorescence changes ΔF/F. In practice, fluorescence measurements are noisy, which was simulated here by adding gaussian-shaped noise. Moreover, signals may be contaminated slightly by neighboring structures.

free calcium following calcium influx. In mathematical terms

$$\Delta[Ca] \alpha \frac{\Delta F}{F} \alpha \frac{1}{1 + \kappa_S + \kappa_{dye}}$$

$$\text{and } \tau \alpha (1 + \kappa_S + \kappa_{dye})$$

Here, we assumed that Δ[Ca] is proportional to the relative fluorescence change ΔF/F, which holds true for small calcium elevations far from dye saturation. Note that ΔF/F further depends on the baseline fluorescence and dynamic range of the indicator type. This discussion leads us to the question: Which dye concentration provides the highest SNR for the measurement of somatic calcium signals? Here, SNR is defined as the ratio of the absolute fluorescence change ΔF and the standard deviation of the baseline fluorescence signal σ_F (FIGURE 4B). In the shot-noise limited case, σ_F equals the square root of the average fluorescence value F, which increases in proportion to the dye concentration (which itself in first approximation is proportional to κ_{dye}). With increasing dye concentration, however, the AP-evoked fluorescence change ΔF follows a saturating function simply because the dye cannot capture more calcium ions than have entered the cell. As a result, the noise level in the ΔF/F traces decreases with dye concentration but also so does the amplitude of the AP-evoked ΔF/F change (FIGURE 4B). It follows

$$\Delta F \alpha \frac{F}{1 + \kappa_S + \kappa_{dye}} \approx \frac{\kappa_{dye}}{1 + \kappa_S + \kappa_{dye}}$$

and for the SNR under shot-noise limited conditions

$$SNR = \frac{\Delta F}{\sigma_F} \alpha \frac{\kappa_{dye}}{(1 + \kappa_S + \kappa_{dye})\sqrt{\kappa_{dye}}} =$$

$$\frac{\sqrt{\kappa_{dye}}}{(1 + \kappa_S + \kappa_{dye})}$$

This dependence of SNR on the calcium indicator concentration is shown in FIGURE 4C. Because of the two opposing effects of reduced noise but larger buffering at higher dye concentration, the curve shows a maximum. The position of the maximum κ_{max} can be found from the first derivative as (3)

$$\kappa_{max} = (1+\kappa_S) \approx \kappa_S$$

where the simplification is justified because typical values of κ_S for cortical pyramidal neurons are 100–150 (21). Hence, the optimal dye concentration is reached when the added calcium buffering capacity equals the endogenous one, a situation termed "balanced loading." For detection of single APs, high-affinity indicators such as Oregon-Green BAPTA-1 (K_D = 0.2–0.3 μM) are required (which, however, might saturate during trains of APs). For such indicators κ_S values of 100–150 for pyramidal neurons correspond to an optimal dye concentration in the range of 25–50 μM. This estimate is close to the estimates for MCBL (20 μM) (51), local electroporation (20 μM) (33), and targeted electroporation (50–250 μM) (34). Note, however, that other cell types, e.g., GABAergic interneurons, may have different requirements because they typically possess a higher endogenous calcium buffering capacity. It is thus worth keeping the simple rule of "balanced loading" in mind and to vary the type of indicator, pipette dye concentration, loading times, or GECI expression levels to optimize the SNR for reconstruction of neuronal spiking activity.

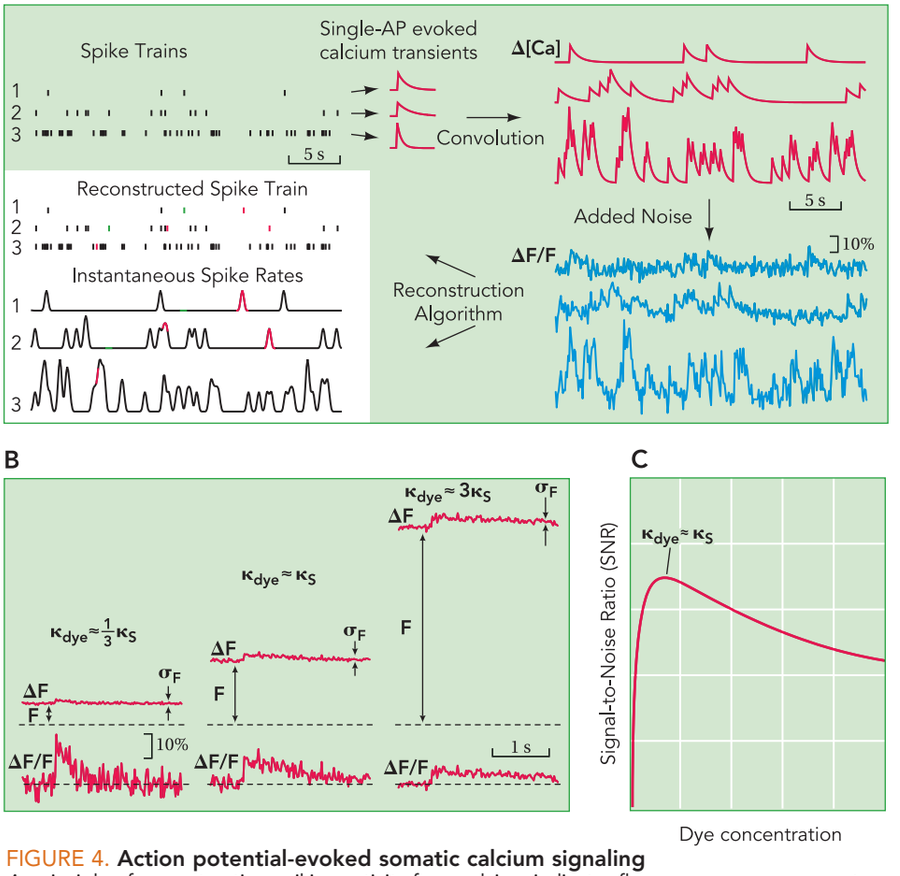

FIGURE 4. **Action potential-evoked somatic calcium signaling**
A: principle of reconstructing spiking activity from calcium indicator fluorescence measurements, exemplified for three simulated neurons. Calcium signals are spike trains convolved by the single AP-evoked calcium transients. From the resulting noisy fluorescence traces (ΔF/F), spiking activity can be reconstructed by estimating either spike times or temporally smoothed instantaneous spike rates. The rate of errors in form of missed spikes (green) or false positives (red) will depend on the noise level. *B*: fluorescence signals depend on the calcium indicator concentration. Here, we simulated single-AP evoked fluorescence signals for three dye-loading conditions with an increasing ratio of κ_{dye} over κ_S. Note that the relative fluorescence change ΔF/F is reduced at higher dye concentration, although ΔF slightly increases. The SNR is given by the ratio of ΔF and σ_F. *C*: dependency of SNR on calcium indicator concentration. A maximal SNR is achieved under "balanced loading" condition, i.e., when the calcium-binding capacity of the indicator κ_{dye} equals the calcium-binding capacity of the endogenous buffers κ_S.

Contamination of Somatic Signals by Neuropil

Another problem one should be aware of, in particular when using MCBL, is that neuropil calcium signals possibly contaminate somatic signals, in the worst case indicating a neuronal spike where none occurred (FIGURE 3D). Although this problem can be reduced by carefully selecting ROIs and restricting the analysis to well focused neurons (25, 50), there is a fundamental aspect to it that relates to the image-formation process in the microscope. Despite "optical sectioning" in 2PLSM, mixing of fluorescence signals can still occur as illustrated in FIGURE 5.

In a simple model of bolus-stained neocortical tissue, we simulated a cell body by a bright sphere embedded in a "sea" of relatively high neuropil background fluorescence (FIGURE 5A). The microscope image of any object is given by the spatial convolution of the object with a characteristic function called the "point spread function" (PSF), which critically depends on the numerical aperture (NA) of the microscope objective. For a two-photon microscope, the two-photon PSF (2P-PSF) is given as the square of the PSF for one-photon excitation (19, 66). To determine the relative contribution of background fluorescence to the cell body signal, we simulated the two-photon images of neuropil and cell body separately by convolving these objects with a theoretical 2P-PSF (19). Remarkably, cross-sectional profiles through the resulting image demonstrate a clear contribution of the neuropil fluorescence to the signal detected within the simulated cell body (FIGURE 5, B AND D). The profiles indicate a strong contamination of the somatic signal at low NAs; but also for relatively high NAs, blurred neuropil fluorescence contributes to the signal at the soma center, where background fluorescence should be lowest. Hence, contamination cannot be neglected, especially since the effectively used NA typically is lower than the NA specified by the manufacturer [which assumes a plane wavefront fill-

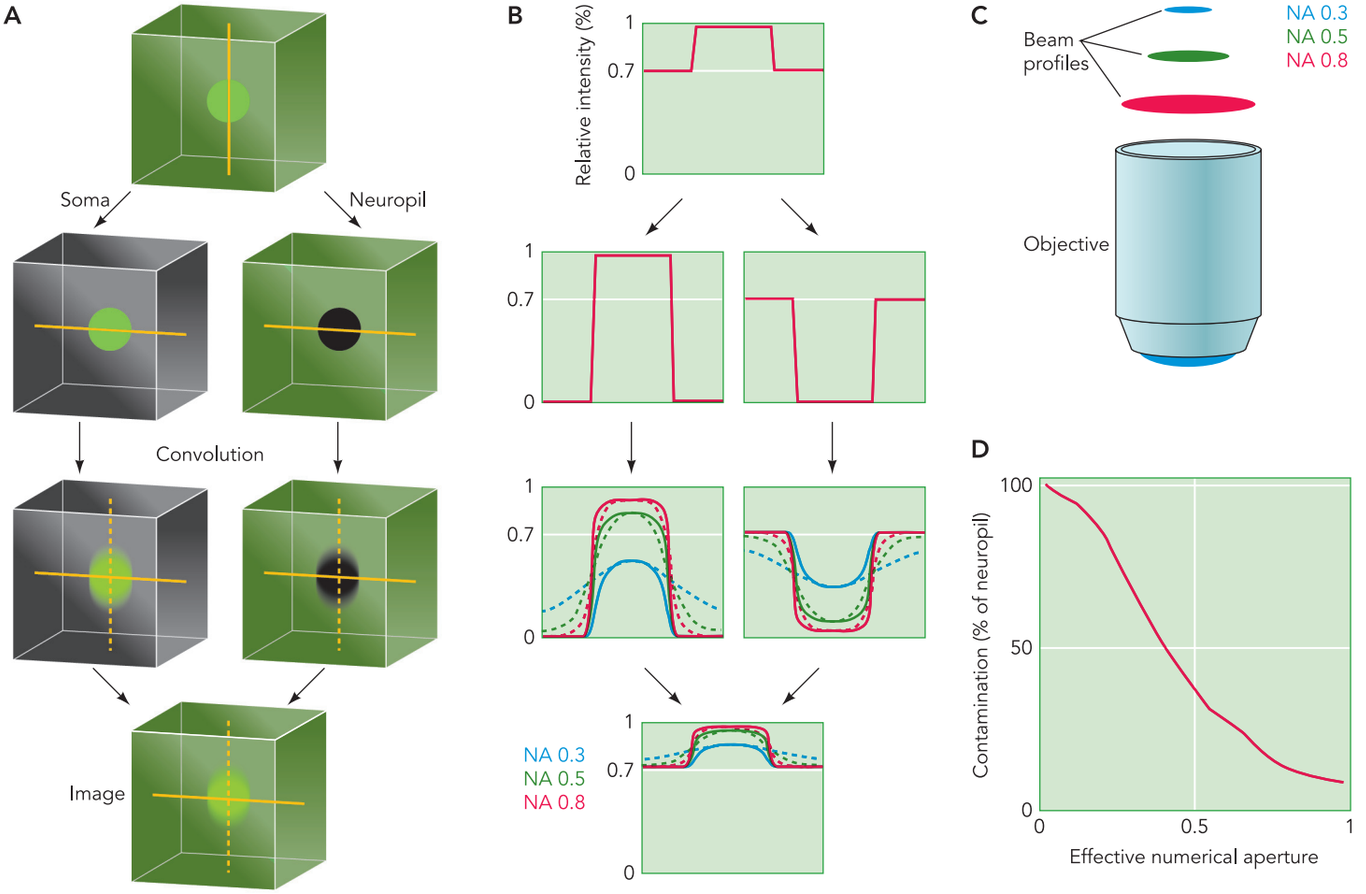

FIGURE 5. **Simulation of neuropil contribution to somatic fluorescence signals.**
Simulation of neuropil contribution to somatic fluorescence signals. A: cell body (16-μm diameter sphere of intensity 1) in a sea of neuropil fluorescence (intensity 0.7, mimicking MCBL loading with Oregon-Green BAPTA-1). 3D images of neuropil and cell body are separately processed by convolving the objects with a theoretical 2P-PSF (shown for NA 0.5). The final image is obtained by a linear superposition of cell body and neuropil images. B: intensity profiles through objects and images for three different NAs along the lateral (solid lines) and axial (broken lines) dimension (corresponding to the yellow lines in A). Note that the intensity level in the center of the final image is a combination of fluorescence from cell body and neuropil. C: the effectively used NA for fluorescence excitation depends on how much the laser beam fills the objective's back aperture. D: dependency of neuropil contamination of somatic calcium signals on effective NA, taking into account fluorescence within a ROI that corresponds to the original cell body diameter. At NA 0.5, about 30% of fluorescence inside the ROI originates from the neuropil, and even for high NAs (0.8-1.0) there is a remaining contribution of around 10%.

ing the entire objective's back-aperture, whereas for in vivo two-photon microscopy the beam profile is Gaussian shaped, and the back-aperture often is under-filled to maximize transmission of excitation light (19)]. Although the problem of contamination cannot be fully overcome, one should therefore aim for an illumination NA as high as possible (trading off against power loss). A good way to verify little contamination is to search for bright neurons that show no somatic signals despite large signals in the surrounding neuropil.

Outlook

In summary, in vivo calcium imaging of network activity creates new opportunities to study the functional architecture of neuronal and glial circuits in the living brain. Further advances in labeling and read-out methods can be expected, especially for fast 3D measurements from large populations. Improved GECIs will facilitate functional measurements from specific sub-networks, and new laser scanning approaches will push current speed limits. Further optimization of fluorescence signals and application of sophisticated signal analysis tools promise reliable single spike detection from large numbers of neurons in 3D. This will allow examination of correlations among individual cells and identification of functionally linked sub-networks that encode specific stimulus features. Moreover, from the reconstructed spiking activity, one can reveal the temporal evolution of the 3D network state, e.g., following sensory stimulation, using advanced analysis tools such as principal component analysis (4). Although most experiments at present are carried out in anesthetized animals, several approaches for imaging in awake behaving animals have been devised that ultimately aim at directly correlating neuronal network dynamics with behavior (1, 9, 20). Finally, through expression of light-activated channel proteins, it might become possible in the future to not only read-out but also control neuronal networks in vivo (2).

Work in the authors' laboratory is supported by the Swiss National Science Foundation, the Human Frontier Science Program Organisation, and the Neuroscience Center Zurich.

References

1. Adelsberger H, Garaschuk O, Konnerth A. Cortical calcium waves in resting newborn mice. *Nat Neurosci* 8: 988–990, 2005.
2. Arenkiel BR, Peca J, Davison IG, Feliciano C, Deisseroth K, Augustine GJ, Ehlers MD, Feng G. In vivo light-induced activation of neural circuitry in transgenic mice expressing channelrhodopsin-2. *Neuron* 54: 205–218, 2007.
3. Borst JG, Helmchen F. Calcium influx during an action potential. *Methods Enzymol* 293: 352–371, 1998.
4. Broome BM, Jayaraman V, Laurent G. Encoding and decoding of overlapping odor sequences. *Neuron* 51: 467–482, 2006.
5. Brustein E, Marandi N, Kovalchuk Y, Drapeau P, Konnerth A. "In vivo" monitoring of neuronal network activity in zebrafish by two-photon Ca^{2+} imaging. *Pflügers Arch* 446: 766–773, 2003.
6. Buzsaki G. Large-scale recording of neuronal ensembles. *Nat Neurosci* 7: 446–451, 2004.
7. Denk W, Strickler JH, Webb WW. Two-photon laser scanning fluorescence microscopy. *Science* 248: 73–76, 1990.
8. Diez-Garcia J, Akemann W, Knöpfel T. In vivo calcium imaging from genetically specified target cells in mouse cerebellum. *Neuroimage* 34: 859–869, 2007.
9. Dombeck DA, Khabbaz AN, Collman F, Tank DW. Imaging large scale neural activity with cellular resolution in awake mobile mice. *Neuron* 56: 43–57, 2007.
10. Garaschuk O, Griesbeck O, Konnerth A. Troponin C-based biosensors: a new family of genetically encoded indicators for in vivo calcium imaging in the nervous system. *Cell Calcium* 42: 351–361, 2007.
11. Garaschuk O, Milos RI, Grienberger C, Marandi N, Adelsberger H, Konnerth A. Optical monitoring of brain function in vivo: from neurons to networks. *Pflügers Arch* 453: 385–396, 2006.
12. Garaschuk O, Milos RI, Konnerth A. Targeted bulk-loading of fluorescent indicators for two-photon brain imaging in vivo. *Nat Protoc* 1: 380–386, 2006.
13. Gelperin A, Flores J. Vital staining from dye-coated microprobes identifies new olfactory interneurons for optical and electrical recording. *J Neurosci Methods* 72: 97–108, 1997.
14. Göbel W, Helmchen F. New angles on neuronal dendrites in vivo. *J Neurophysiol*. In press. doi:10.1152/jn.00850.02007 2007.
15. Göbel W, Kampa BM, Helmchen F. Imaging cellular network dynamics in three dimensions using fast 3D laser scanning. *Nat Methods* 4: 73–79, 2007.
16. Hammond AT, Glick BS. Raising the speed limits for 4D fluorescence microscopy. *Traffic* 1: 935–940, 2000.
17. Hasan MT, Friedrich RW, Euler T, Larkum ME, Giese G, Both M, Duebel J, Waters J, Bujard H, Griesbeck O, Tsien RY, Nagai T, Miyawaki A, Denk W. Functional fluorescent Ca^{2+} indicator proteins in transgenic mice under TET control. *PLoS Biol* 2: e163, 2004.
18. Heim N, Garaschuk O, Friedrich MW, Mank M, Milos RI, Kovalchuk Y, Konnerth A, Griesbeck O. Improved calcium imaging in transgenic mice expressing a troponin C-based biosensor. *Nat Methods* 4: 127–129, 2007.
19. Helmchen F, Denk W. Deep tissue two-photon microscopy. *Nat Methods* 2: 932–940, 2005.
20. Helmchen F, Fee MS, Tank DW, Denk W. A miniature head-mounted two-photon microscope. High-resolution brain imaging in freely moving animals. *Neuron* 31: 903–912, 2001.
21. Helmchen F, Imoto K, Sakmann B. Ca^{2+} buffering and action potential-evoked Ca^{2+} signaling in dendrites of pyramidal neurons. *Biophys J* 70: 1069–1081, 1996.
22. Helmchen F, Waters J. Ca^{2+} imaging in the mammalian brain in vivo. *Eur J Pharmacol* 447: 119–129, 2002.
23. Hirase H, Qian L, Bartho P, Buzsaki G. Calcium dynamics of cortical astrocytic networks in vivo. *PLoS Biol* 2: E96, 2004.
24. Iyer V, Hoogland TM, Saggau P. Fast functional imaging of single neurons using random-access multiphoton (RAMP) microscopy. *J Neurophysiol* 95: 535–545, 2006.
25. Kerr JN, de Kock CPJ, Greenberg DS, Bruno RM, Sakmann B, Helmchen F. Spatial organization of neuronal population responses in layer 2/3 of rat barrel cortex. *J Neurosci*. In press.
26. Kerr JN, Greenberg D, Helmchen F. Imaging input and output of neocortical networks in vivo. *Proc Natl Acad Sci USA* 102: 14063–14068, 2005.
27. Knöpfel T, Diez-Garcia J, Akemann W. Optical probing of neuronal circuit dynamics: genetically encoded versus classical fluorescent sensors. *Trends Neurosci* 29: 160–166, 2006.
28. Kotlikoff MI. Genetically encoded Ca^{2+} indicators: using genetics and molecular design to understand complex physiology. *J Physiol* 578: 55–67, 2007.
29. Kreitzer AC, Gee KR, Archer EA, Regehr WG. Monitoring presynaptic calcium dynamics in projection fibers by in vivo loading of a novel calcium indicator. *Neuron* 27: 25–32, 2000.
30. Lin BJ, Chen TW, Schild D. Cell type-specific relationships between spiking and $[Ca^{2+}]_i$ in neurons of the *Xenopus* tadpole olfactory bulb. *J Physiol* 582: 163–175, 2007.
31. Miesenböck G, Kevrekidis IG. Optical imaging and control of genetically designated neurons in functioning circuits. *Annu Rev Neurosci* 28: 533–563, 2005.
32. Mrsic-Flogel TD, Hofer SB, Ohki K, Reid RC, Bonhoeffer T, Hübener M. Homeostatic regulation of eye-specific responses in visual cortex during ocular dominance plasticity. *Neuron* 54: 961–972, 2007.
33. Nagayama S, Zeng S, Xiong W, Fletcher ML, Masurkar AV, Davis DJ, Pieribone VA, Chen WR. In vivo simultaneous tracing and Ca^{2+} imaging of local neuronal circuits. *Neuron* 53: 789–803, 2007.
34. Nevian T, Helmchen F. Calcium indicator loading of neurons using single-cell electroporation. *Pflügers Arch* 454: 675–688, 2007.
35. Nguyen QT, Callamaras N, Hsieh C, Parker I. Construction of a two-photon microscope for video-rate Ca^{2+} imaging. *Cell Calcium* 30: 383-393, 2001.
36. Niell CM, Smith SJ. Functional imaging reveals rapid development of visual response properties in the zebrafish tectum. *Neuron* 45: 941-951, 2005.
37. Nimmerjahn A, Kirchhoff F, Kerr JN, Helmchen F. Sulforhodamine 101 as a specific marker of astroglia in the neocortex in vivo. *Nat Methods* 1: 31-37, 2004.
38. O'Donovan MJ, Bonnot A, Wenner P, Mentis GZ. Calcium imaging of network function in the developing spinal cord. *Cell Calcium* 37: 443-450, 2005.

39. O'Donovan MJ, Ho S, Sholomenko G, Yee W. Real-time imaging of neurons retrogradely and anterogradely labelled with calcium-sensitive dyes. *J Neurosci Methods* 46: 91-106, 1993.

40. Ohki K, Chung S, Ch'ng Y, Kara P, Reid R. Functional imaging with cellular resolution reveals precise micro-architecture in visual cortex. *Nature* 433: 597-603, 2005.

41. Ohki K, Chung S, Kara P, Hubener M, Bonhoeffer T, Reid RC. Highly ordered arrangement of single neurons in orientation pinwheels. *Nature* 442: 925-928, 2006.

42. Pologruto TA, Yasuda R, Svoboda K. Monitoring neural activity and [Ca^{2+}] with genetically encoded Ca^{2+} indicators. *J Neurosci* 24: 9572-9579, 2004.

43. Ramdya P, Reiter B, Engert F. Reverse correlation of rapid calcium signals in the zebrafish optic tectum in vivo. *J Neurosci Methods* 157: 230-237, 2006.

44. Reddy GD, Saggau P. Fast three-dimensional laser scanning scheme using acousto-optic deflectors. *J Biomed Opt* 10: 64038, 2005.

45. Ross WN, Nakamura T, Watanabe S, Larkum M, Lasser-Ross N. Synaptically activated Ca^{2+} release from internal stores in CNS neurons. *Cell Mol Neurobiol* 25: 283–295, 2005.

46. Rozsa B, Katona G, Vizi ES, Varallyay Z, Saghy A, Valenta L, Maak P, Fekete J, Banyasz A, Szipocs R. Random access three-dimensional two-photon microscopy. *Appl Opt* 46: 1860–1865, 2007.

47. Salome R, Kremer Y, Dieudonne S, Leger JF, Krichevsky O, Wyart C, Chatenay D, Bourdieu L. Ultrafast random-access scanning in two-photon microscopy using acousto-optic deflectors. *J Neurosci Methods* 154: 161–174, 2006.

48. Sato TR, Gray NW, Mainen ZF, Svoboda K. The functional microarchitecture of the mouse barrel cortex. *PLoS Biol* 5: e189, 2007.

49. Smetters D, Majewska A, Yuste R. Detecting action potentials in neuronal populations with calcium imaging. *Methods* 18: 215–221, 1999.

50. Sohya K, Kameyama K, Yanagawa Y, Obata K, Tsumoto T. GABAergic neurons are less selective to stimulus orientation than excitatory neurons in layer II/III of visual cortex, as revealed by in vivo functional Ca^{2+} imaging in transgenic mice. *J Neurosci* 27: 2145–2149, 2007.

51. Stosiek C, Garaschuk O, Holthoff K, Konnerth A. In vivo two-photon calcium imaging of neuronal networks. *Proc Natl Acad Sci USA* 100: 7319–7324, 2003.

52. Sullivan MR, Nimmerjahn A, Sarkisov DV, Helmchen F, Wang SSH. In vivo calcium imaging of circuit activity in cerebellar cortex. *J Neurophysiol* 94: 1636–1644, 2005.

53. Svoboda K, Denk W, Kleinfeld D, Tank DW. In vivo dendritic calcium dynamics in neocortical pyramidal neurons. *Nature* 385: 161–165, 1997.

54. Svoboda K, Yasuda R. Principles of two-photon excitation microscopy and its applications to neuroscience. *Neuron* 50: 823–839, 2006.

55. Takano T, Han X, Deane R, Zlokovic B, Nedergaard M. Two-photon imaging of astrocytic Ca^{2+} signaling and the microvasculature in experimental mice models of Alzheimer's disease. *Ann NY Acad Sci* 1097: 40–50, 2007.

56. Takano T, Tian GF, Peng W, Lou N, Libionka W, Han X, Nedergaard M. Astrocyte-mediated control of cerebral blood flow. *Nat Neurosci* 9: 260–267, 2006.

57. Tamamaki N, Yanagawa Y, Tomioka R, Miyazaki J, Obata K, Kaneko T. Green fluorescent protein expression and colocalization with calretinin, parvalbumin, and somatostatin in the GAD67-GFP knock-in mouse. *J Comp Neurol* 467: 60–79, 2003.

58. Tian GF, Azmi H, Takano T, Xu Q, Peng W, Lin J, Oberheim N, Lou N, Wang X, Zielke HR, Kang J, Nedergaard M. An astrocytic basis of epilepsy. *Nat Med* 11: 973–981, 2005.

59. Tian GF, Takano T, Lin JH, Wang X, Bekar L, Nedergaard M. Imaging of cortical astrocytes using 2-photon laser scanning microscopy in the intact mouse brain. *Adv Drug Delivery Res* 58: 773–787, 2006.

60. Tsien RY. A non-disruptive technique for loading calcium buffers and indicators into cells. *Nature* 290: 527–528, 1981.

61. Wachowiak M, Cohen LB. Representation of odorants by receptor neuron input to the mouse olfactory bulb. *Neuron* 32: 723–735, 2001.

62. Wang X, Lou N, Xu Q, Tian GF, Peng WG, Han X, Kang J, Takano T, Nedergaard M. Astrocytic Ca^{2+} signaling evoked by sensory stimulation in vivo. *Nat Neurosci* 9: 816–823, 2006.

63. Wong RO. Calcium imaging and multielectrode recordings of global patterns of activity in the developing nervous system. *Histochem J* 30: 217–229, 1998.

64. Yaksi E, Friedrich RW. Reconstruction of firing rate changes across neuronal populations by temporally deconvolved Ca^{2+} imaging. *Nat Methods* 3: 377–383, 2006.

65. Yaksi E, Judkewitz B, Friedrich RW. Topological reorganization of odor representations in the olfactory bulb. *PLoS Biol* 5: e178, 2007.

66. Zipfel WR, Williams RM, Webb WW. Nonlinear magic: multiphoton microscopy in the biosciences. *Nat Biotechnol* 21: 1369–1377, 2003.